Modeling Approach To Assess Clustering Impact on Release Rates of Pesticides from Microencapsulated Products

STEVEN A. CRYER* AND STEPHEN L. WILSON

Dow AgroSciences, LLC, 9330 Zionsville Road, Indianapolis, Indiana 46268

The pesticide release rate from polymer-encapsulated microcapsules is controlled by diffusion across the polymer membrane, membrane thickness, and pesticide loading. However, conditions for microcapsule clustering following conventional application practices and the impact of clustering on the overall release rate are often ignored. Microcapsules are delivered to target surfaces using water droplets as a carrier, and capillary-driven velocities arise within the deposited sessile drop as the water evaporates. This work describes experimental observations and a quasi-static mathematical approach used to elucidate microcapsule clusters that remain following the drop-drying process, along with the anticipated patterns for pesticide release as a function of cluster geometries. The dynamic behavior of a drying sessile drop was modeled as a trajectory of constrained quasi-static equilibrium shapes having a fixed contact line. Observed monolayer clustering of microcapsules was a function of the initial contact angle and size of the sessile drop, evaporation rate, and the microcapsule number density within the drop. The net pesticide release rate from microcapsule clusters was calculated from superposition of smaller decomposed cluster geometries for which release rates were determined by numerical solution to the mass balance governing equation, thereby coupling the self-assembly of microcapsule and microcapsule clustering with environmental release rate predictions.

KEYWORDS: Microencapsulation; clustering; diffusion; release rate; sessile drop; self-assembly; contact line pinning

INTRODUCTION

An indirect measure of pesticide efficacy is the product of contact time and environmental concentration. Environmental concentrations have to be high enough over a sufficient time frame to affect pests while simultaneously undergoing environmental degradation processes that reduce the environmental concentration. The contact time for pest control can be small if the pesticide degrades rapidly, and microencapsulation is advantageously used to create an effective active duration time frame that is longer than the degradation half-life of the pure pesticide alone (*1*, *2*). Multiple reviews of polymer-encapsulated agrochemicals exist (*3*−*5*), along with many studies documenting pesticide release rates from microcapsules (*6*−*12*).

Microcapsule Release Rates. Conventional microencapsulation incorporates a polymer membrane around the pesticide (**Figure 1**), with the pesticide release controlled by diffusion across the membrane (*13*).

GLOSSARY

a = capsule radius [cm]
C = concentration of pesticide within the capsule (assumed to be uniform throughout the capsule) [g cm^{-3}]
C_0 = initial concentration of pesticide within the capsule for $t \leq 0$ [g cm^{-3}]

C_s = concentration of pesticide at the membrane−environmental interface [g cm^{-3}]
C_∞ = concentration of pesticide within the environment that is not affected by the contribution from the capsule (typically equal to zero) [g cm^{-3}]
C_{ext} = concentration of active pesticide outside the membrane wall and within the environment [g cm^{-3}]
h = membrane thickness [cm]
L = characteristic length scale for resistance to mass transfer within the environmental matrix, where $C_{ext} \sim C_\infty$ [cm]
M = mass of pesticide within capsule ($C \times V$) [g]
M_0 = initial mass of pesticide within the capsule for $t \leq 0$ [g]
t = time [s]
V = volume of spherical capsule [cm^3]
D_m = diffusion coefficient of pesticide in polymer matrix [cm^2 s^{-1}]
D_{env} = diffusion coefficient of pesticide in the environment [cm^2 s^{-1}]
$\alpha = \frac{D_m}{D_{env}} \frac{L}{h}$

Analytical solutions to the one-dimensional diffusion equation in spherical coordinates for diffusion transport across this polymer layer for a variety of different boundary conditions are summarized elsewhere (*14*−*17*), and when $C_\infty = 0$, the time (t)-dependent solution becomes

$$\frac{C}{C_0} = \frac{M}{M_0} = e^{-0.693t/\tau} \qquad (1)$$

*Corresponding author (e-mail sacryer@dow.com).

5444   *J. Agric. Food Chem.*, Vol. 57, No. 12, 2009
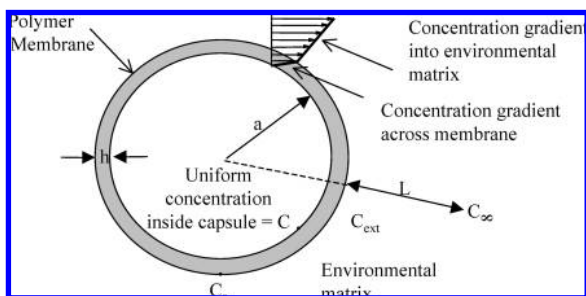
Cryer and Wilson

Figure 1. Idealized geometry of a spherical capsule.

where τ is the characteristic half-life for release

$$\tau = 0.693 \frac{ah(1+\alpha)}{3D_m} \tag{2}$$

Mass (M) and concentration (C) are often used interchangeably when the volume (V) of a capsule remains constant over time (e.g., mass equals the product of concentration and volume).

The mass of pesticide that has left the capsule (M_r) at any time is (*18*)

$$M_r = M_0(1 - e^{-0.693t/\tau}) \tag{3}$$

Environmental degradation mechanisms occur once the pesticide is outside the capsule. Assuming first-order kinetic processes for release rate and environmental degradation of the pesticide parametrized by the rate constant k, the mass of active pesticide outside the capsule (R) can be expressed as

$$\frac{R}{M_0} = \frac{1}{\left(\frac{\tau}{\tau_0} - 1\right)} e^{-0.693(\tau/\tau_0)(t/\tau)} \{e^{0.693(\tau/\tau_0 - 1)t/\tau} - 1\} \tag{4}$$

where

$$\tau_0 = \frac{0.693}{k}$$

Here, τ_0 is the degradation half-life of the active ingredient within the environment with k the assumed first-order, lumped sum kinetic degradation rate constant. The ratio τ/τ_0 governs the relative importance of diffusion versus environmental degradation time scales.

More complex modeling algorithms have been proposed to express pesticide loss from single microcapsules as a function of polymer properties and solubility of the pesticide within the oil phase being encapsulated (*19−21*). However, what are lacking in historical works are the interactions of neighboring microcapsules to the overall release rate.

Microcapsule Clustering. The release rate of pesticide from microcapsules into the environment slows as the concentration driving force for mass transfer decreases (e.g., density of neighboring capsules increases). Clustering of solid particles can occur in two phase systems (liquid, solids) in which one phase (liquid) is responsible for transport of the second phase (solids). The phenomenon of the "coffee ring" where macroscopic patterns of fine particles arise as a drop containing the particles evaporates was first explained by Deegan et al. (*22*), who assumed vapor transport was rate limiting. Numerical solutions are also summarized (*23, 24*). Solid particle clustering was further quantified by alternative mechanisms dictated by hydrodynamics of the liquid phase (*25*). Solids within the drop are transported to the drop contact line by capillary induced convective flow patterns, thus forming annular rings of solid material upon drop

evaporation and providing a mechanism to organize suspended particles that range from nanometers to micrometers (*26, 27*). Capillary-induced convection in a pinned sessile drop (drop resting on a solid surface) has been used to optimize ink jet printing, to create self-assembling micro- and nanostructures (*28, 29*), and in understanding the crystalline patterns that form following the drying of droplets of DNA which are stretched and subsequently deposited for gene expression profiling (*30*). Additionally, the impact of Marangoni (surface tension gradients) at the drop interface can reverse the formation of the "coffee-ring" deposits (*31*).

Sessile Drop Equilibrium Shapes. Drops of liquid on a solid surface seek to minimize the drop surface energy, with the drop contact angle governing the shape of a liquid against a solid. Energy minimization for axi-symmetric drops at equilibrium is given by the Laplace equation of capillarity. The dimensionless Bond number (Bo) arises in fluid mechanics as a measure of the ratio of body forces (gravity) to surface tension. Gravity effects are considered to be negligible when Bo $\ll$ 1.

Velocity Patterns in Evaporating Drop. Understanding how microcapsules move and ultimately cluster is a mandatory precursor in understanding environmental release rates for pesticides. A unidirectional, one-dimensional radial flow from the drop center to the drop edge was suggested as being responsible for the clustering of solid particles near the pinned, wetted perimeter, assuming lubrication theory, and evaporation was described by a Laplace equation (*22, 32−34*). There is a singularity at $r = a$ (at the wetted perimeter) where the velocity $\rightarrow \infty$.

$$V_r = \frac{a^2}{4(t_f - t)r} \left\{ \frac{1}{\sqrt{1 - \left(\frac{r}{a}\right)^2}} - \left[1 - \left(\frac{r}{a}\right)^2 \right] \right\} \tag{5}$$

GLOSSARY

a = radius of the pinned, wetted perimeter
r = radial direction from the center of the drop ($r = 0$ at center, $r = R$ at pinned perimeter)
t = time following the drop formation
t_f = final time post drop formation when the drop has fully evaporated

A two-dimensional analytical expression for the hydrodynamic potential inside an evaporating spherical sessile drop with a pinned contact line (wetted perimeter of liquid on solid surface) that does not give rise to a singularity at the drop edge has also been proposed. Equations 6−8 represent the Fourier−Legendre series expansion describing the velocity potential within the evaporating drop (*35*).

$$\phi(r,\varphi) = \sum_{k=0}^{\infty} A_k \left(\frac{r}{R}\right)^k P_k(\cos\varphi) \tag{6}$$

$$\frac{\partial \phi(r,\varphi)}{\partial r} = \sum_{k=0}^{\infty} k \left(\frac{A_k}{R^k}\right) r^{k-1} P_k(\cos\varphi) \tag{7}$$

$$A_{2k} = u_0 R(4k+1) \frac{(-1)^k (2k-2)!}{2^{2k} k! (k+1)!} \tag{8}$$

GLOSSARY

$P_k(\cos\varphi)$ = Legendre polynomials
u_0 = dh/dt, the rate of change in the spherical cap height with respect to time [cm s^{-1}]

The flow profile within the liquid drop was calculated from the velocity potential [$\phi(r,\varphi)$] once the drop dimensions and the rate of change of the drop height with time (u_0) are known. Both drop dimensions and u_0 were measured experimentally for this work.

MATERIALS AND METHODS

A combined experimental and numerical approach was used to understand and predict conditions when pesticide release rates from microcapsules can be altered only on the basis of capsule clustering. The computational fluid dynamics (CFD) software package Fluent 6.3 (*36*) was used to explore flow patterns resulting from momentum transfer from a falling drop impacting a solid surface and in pesticide mass transport from clusters of microcapsules. Fluent is a segregated-implicit, coupled-explicit/implicit finite volume method capable of solving the continuity, momentum, and energy conservation equations.

Capsule Release Rate Approximations. CFD mass conservation equation (diffusion) was used to predict pesticide mass transfer losses for seven specific clustered microcapsule geometries (**Figure 2**). Only the immediate adjacent capsules were considered in the analysis, thus providing a bound for higher release rate predictions. The darker shaded capsule is the capsule of interest. Each capsule was assumed to have similar properties (i.e., radius, mass loading, membrane thickness, and so on). Unsteady mass transfer simulations were performed for the geometries represented in **Figure 2**, with the mass of pesticide remaining within the central capsule calculated over time.

Cluster geometries were developed using an empirical random placement approach. The number of individual microcapsules in a cluster (N_T) was defined by a probability density function (PDF) based upon experimental observations. The cluster was randomly grown as illustrated in **Figure 3** with N_T selected by Monte Carlo (MC) sampling of the PDF. The starting capsule of a cluster was placed at the origin (0,0). There are four possible locations for the next capsule [(−1, 0), (0, 1), (1,0), (0,−1)]. Each possibility has the same probability of being randomly selected for the next capsule location. For this example, the nodal point (1,0) was chosen for the next capsule placement (**Figure 3b**). Now, there are six distinct locations where the next capsule can be randomly placed as illustrated by the gray
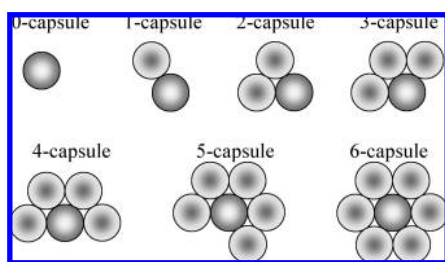

Figure 2. Single capsule surrounded by up to six additional capsules.

nodes in **Figure 3b**. The procedure was numerically repeated until N_T capsules are contained in the cluster. Each capsule within the two-dimensional cluster has a characteristic number of surrounding capsules. Release for any monolayer capsule cluster was approximated on the basis of the decomposed cluster structures (e.g., **Figure 2**) and a weighted linear superposition for all 0−6 subcapsule geometries represented.

A 17-cluster example is provided in **Figure 4**, illustrating the locations for the 3 unique capsules surrounded by 6 neighboring capsules contained within this unique cluster. Each capsule within the cluster was evaluated for neighbors, and the capsule net rate constant for pesticide release was assumed to be a linear weighting of release rate constants for the smaller decomposed capsule geometries (e.g., **Figure 2**)

$$k_{\text{net}} = \frac{1}{N_T} \sum_{i=1}^{6} N_i k_i \qquad (9)$$

Here, N_i is the total number of unique decomposed capsule geometries having "*i*" surrounding capsules in the cluster, and k_i represents the release rate constant for the decomposed capsule cluster geometry "*i*" determined from CFD.

An entire two-dimensional cluster can be disseminated into unique numbers of individual 0-, 1-, 2-, 3-, 4-, 5-, and 6-capsule interaction-component building blocks of known CFD predicted release profiles. The overall mass loss from the clusters varies depending upon physical properties of the capsule and pesticide (e.g., eqs 1−3) and cluster orientation and geometry because different cluster orientations (for a fixed N_T) have different fractions of 0−6 capsule interactions.

Visualization System for Clustering. Water drops (0.5−5 μL) containing microcapsules were placed on glass slides using a 10 μL syringe. Drop evaporation and microcapsule clustering following evaporation were analyzed using an Olympus Privis AX70 microscope with 10×, 20×, 40×, 60×, and 100× optics and a Sony 3CCD color video camera (model DXC-970MD). A TA Instruments TGA 2050 (thermal gravimetric analyzer) was used to measure water drop evaporation rates. Multiple replications for room temperature evaporative mass losses for several sizes of distilled water droplets (1, 5 μL) were measured. Drop volumes were representative of volumes anticipated from agricultural spray nozzles.

Microcapsules. Microcapsules were prepared by interfacial/condensation polymerization where the membrane wall was formed by the reaction of polymethylene polyphenylisocyanate (PAPI 27, Dow Chemical; oil-soluble monomer) with diethylenetriamine (DETA; water-soluble monomer) to form a polyurea. Cross-linking can occur because both monomers contain greater than two reacting groups per molecule. The oil used was Aromatic 100 without any dissolved pesticide to produce "blank" microcapsules. Differing amounts of mixing shear were performed to create an emulsion (water, surfactant, solvent (oil), and oil soluble monomer) having different size distributions, and subsequent polymerization occurs when the water-soluble monomer was added. A Malvern Instruments Mastersizer 2000 particle size analyzer was used to record the capsule size distributions for the formulations used in this analysis. Two different size distributions (μ = 2 or 10 μm, respectively) were created to
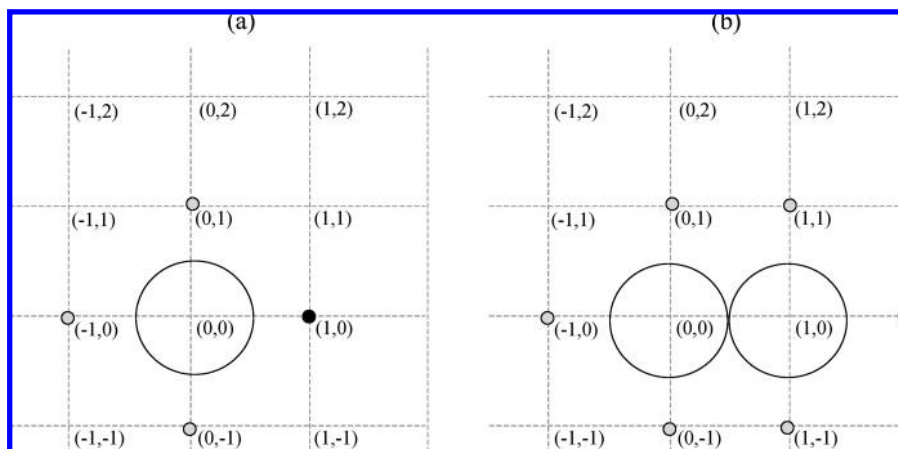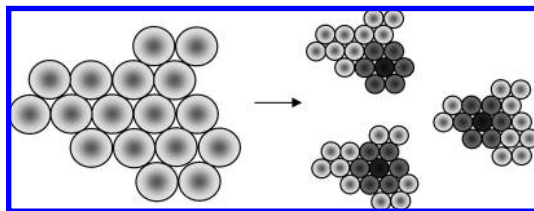

Figure 3. Two-dimensional cluster formation based upon random placement of capsules with spatial coordinates scaled by the microcapsule diameter.

Figure 4. Decomposition example for 17-capsule cluster into a number of capsules surrounded by 6 neighbors.

Figure 5. Force balance on an individual microcapsule in two-phase shear flow.

Figure 6. Geometrical constraints for a sphere of radius *R*. *h* is the height of the spherical cap used to approximate the evaporating sessile drop.

approximate size distributions associated with commercial agricultural formulation microcapsules.

Capsule Velocity Measurements. Velocity magnitudes for microcapsule migration during drop evaporation were estimated using video clips. The video clip was run over a 10 s interval (24 images per second), and individual particles isolated in the 0 s hardcopy frame were tracked to the stopping point of the 10 s frame on the computer screen. Distance measurements from the starting point to the ending point over the 10 s time period provide estimates of the velocity magnitude. Twelve particles were tracked in each experiment to address velocity variability.

Theoretical Considerations. A force balance on an individual capsule within a flow regime yields insight into important transport mechanisms (**Figure 5**). A friction force arises if a microcapsule is touching the solid substrate. However, this force was considered to be negligible as long as there was a thin film of fluid between the microcapsule and solid substrate. In addition, a surface tension force arises if the capsule extends out of the drop and into the air. This force is only manifested when the thickness of the drop is of the same magnitude as the microcapsule diameter. The shear and drag force are driven by the capillary-induced velocity profile set up within the evaporating drop. When all forces balance, the microcapsule remains stationary.

The drop liquid/vapor interface location was solved numerically using the program Surface Evolver (*37*) for the sessile drop shape. Surface Evolver generates equilibrium shapes for a given volume of liquid and a known contact angle with the solid substrate. A quasi-static description/approximation was introduced for the dynamic states.

Approximations Using a Spherical Hemisphere. The sessile drop was considered to be spherical because the gravitational effect on small droplets on the order of 5 μL was negligible (Bo ≪ 1). In this nomenclature of **Figure 6**, *x* is the radius of the contact perimeter, *h* is the height of the spherical cap, and *R* is the radius of the sphere used to describe the drop. The value of *x* remains constant for a pinned contact line, and only the values of θ, *h*, and *R* change as the carrier drops evaporate. Geometric constraints dictate that

$$h = R(1 - \cos \theta) \tag{10}$$

$$x \equiv R \sin \theta = R_0 \sin \theta_0 \tag{11}$$

and that time is scaled by volume changes. Thus

$$\frac{t}{t_f} = 1 - \frac{V}{V_0} \tag{12}$$

where t_f = time when all of the liquid within the drop has evaporated, and the volume of spherical cap (*V*) is

$$V = \frac{1}{3}\pi h^2 (3R - h) = \frac{\pi}{3} R^3 (1 - \cos \theta)^2 (2 + \cos \theta) \tag{13}$$

The initial parameters (V_0, R_0, h_0, θ_0) denoting the drop shape at the onset of evaporation (e.g., stationary drop immediately following placement on a solid substrate) were assumed to be known via solutions by the program Solver Evolver or the spherical cap assumption.
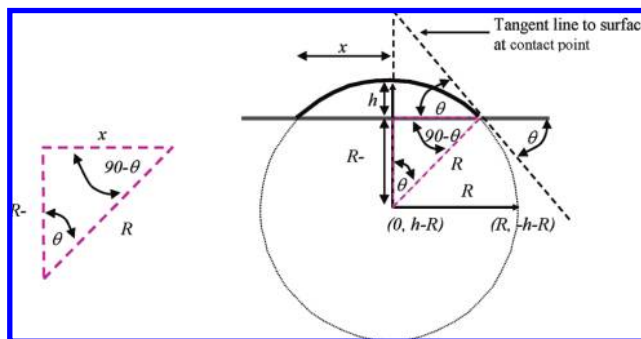
GLOSSARY

V_0 = volume of the drop at time = 0
R_0 = radius of sphere describing drop (spherical cap) at time = 0
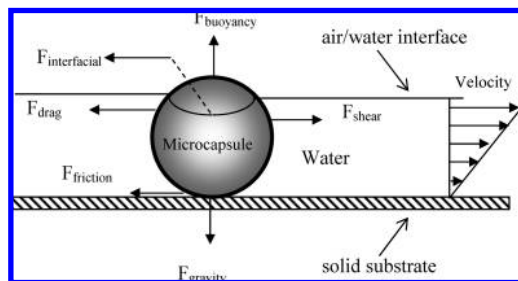
h_0 = height of spherical cap at time = 0
θ_0 = contact angle of drop at time = 0

Microcapsule Transport via Convective Patterns from Evaporation. The modeling system simulates the dynamic behavior (shape) of a drying sessile drop as a trajectory of constrained equilibria. Velocity magnitudes (F_{flow}) were approximated by the Laplace flow generated within the drop (pinned contact line) as it evaporates (*35*). The flow components were derived within the spherical cap once the drop shape was known. Microcapsule trajectories within this flow field were coupled with the vertical buoyancy/gravity components for the microcapsule to yield the microcapsule trajectory within the flow field. A neutrally buoyant capsule will follow the flow streamlines, whereas a capsule having a bulk density greater or less than that of the carrier will generate patterns that deviate from the flow streamlines. It was assumed that microcapsules do not significantly alter the underlying base flow that was derived for a single phase fluid.

Force balances for the microcapsules ($F_{x|new}$, $F_{y|new}$) in the (x, y) directions, respectively, were performed to estimate the new trajectory of the microcapsule at each quasi-static time step ($0 \leq t \leq t_f$). It is inherently implied that the form and friction drag on the capsule in the flow field are approximated by low Reynolds number approximations.

$$F_{y|new} = F_{gravity} - F_{buoyancy} + F_{flow} \sin \theta =$$
$$\frac{4}{3}\pi R_{cap}^3 (\rho_{cap} - \rho_{fluid})g + 6\pi R_{cap} v_\infty \sin \theta \tag{14}$$

$$F_{x|new} = 6\pi \mu R_{cap} v_\infty \cos \theta \tag{15}$$

$$\Theta = \text{trajectory angle} = \frac{F_{x|new}}{F_{y|new}} \tag{16}$$

$$v_\infty = (v_x^2 + v_y^2)^{1/2} \tag{17}$$

Article

J. Agric. Food Chem., Vol. 57, No. 12, 2009   **5447**

Table 1. Fit of CFD Results Using Geometries of **Figure 2** to a First-Order Exponential Decay Model[a]

no. of surrounding capsules (i)	k_i (day^{-1})	r^2
0	0.1467	0.8385
1	0.1168	0.7951
2	9.30E−02	0.7663
3	7.83E−02	0.7772
4	6.90E−02	0.7971
5	6.24E−02	0.8251
6	5.58E−02	0.8574

[a] $M/M_0 = e^{-kt}$, where t is in days.

where v_x and v_y are velocity components in the x and y directions, respectively, and R_{cap} equals the microcapsule radius.

Contact Line Pinning. Most prior work assumes the sessile drop has a pinned contact line (*22−24, 32−35*). Little work has been performed to understand why/how a contact line of a sessile drop becomes pinned when solid particles are present. Transient flow patterns within the liquid following a 5 μL water drop impact on solid surfaces when released from a height of 50 μm were determined by CFD.

RESULTS AND DISCUSSION

Computational Fluid Dynamics. *Release Rate Approximations.* Results of CFD predicted release rates of decomposed 0−6 surrounding capsule clusters follow an exponential decay pattern with time and are summarized in **Table 1**. Next, another simple exponential function (eq 18, $r^2 = 0.97$) was found to adequately represent the correlation between the number of capsules within a cluster and the scaled mass loss rate constant for a specific capsule (k_i/k_0).

$$k_i/k_0 = \exp[-0.187 \times S_i] \qquad (18)$$

S_i equals the integer number of surrounding capsules (integer value between 0 and 6, inclusive) because a single capsule rate constant (k_0) was theoretically known and a function of polymer properties and membrane thickness (eq 2 when characteristic half-life is converted to a rate constant). Thus, different polymers and membrane thicknesses can be assumed, k_0 updated, and eq 18 used to estimate release losses as the number of surrounding capsules increases. **Figure 7** illustrates results for a 17-capsule cluster using the proposed decomposition approach for the mass fraction of pesticide remaining within the capsule over time.

Droplet Impact on Solid Surface. CFD-predicted velocity patterns within the drop and surrounding air were calculated as the water drop impacts the solid surface, rebounds, and transfers momentum until viscous dissipation within the drop brings the drop to rest (**Figure 8**). Velocity vectors at impact indicate a strong driving force to the perimeter edge. Although these simulations do not include any solid particles, flow patterns indicate capsules were driven to the wetted perimeter of the drop before the drop comes to a full resting position. It was postulated that the nearly instantaneous onset of capsules at the perimeter pins and fixes the contact line as the sessile drop attains its initial equilibrium shape.

Experimental Observations. *Microcapsule Size.* Microcapsule size distributions for the 2 and 10 μm blank formulations used for experimental observations illustrate multimodal behavior (**Figure 9**). Distribution means were close to the target values of 2 and 10 μm, respectively.

Capsule Clustering. Qualitative Observations. By visual observation, the contact line for a water droplet containing microcapsules was indeed pinned during the entire evaporation process. Also, there was always a higher percentage of smaller
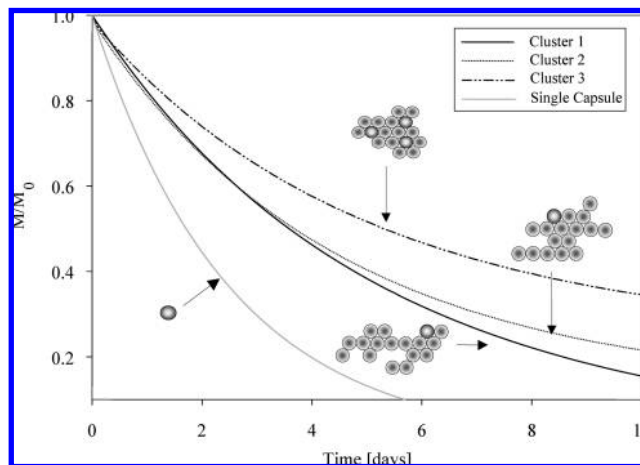

Figure 7. Representative release loss from three different 17-capsule clusters. Physical properties for capsules are identical [only difference is in cluster structure, $k_0 = 0.405$ day^{-1} (k_0 is the release coefficient for a single capsule in an infinite medium)].
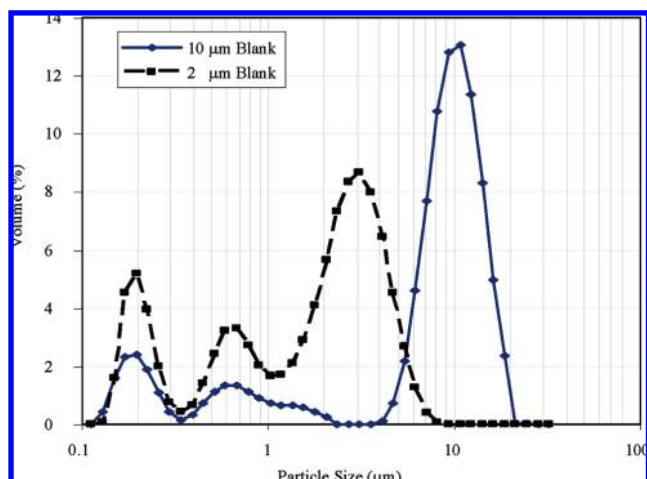
diameter capsules observed near the perimeter edge after evaporation (**Figure 10**). Similarly, there was a higher percentage of larger diameter capsules away from perimeter edge (combination of large and small capsules with microcapsules apparently segregated by size as one travels from the wetted perimeter edge toward the center of the wetted area. Of interest was the fact that indeed a "doughnut" shape of a single layer thickness of microcapsules forms following evaporation of the water carrier. Only single layers of capsules (eg., a monolayer of two dimensions) were observed for all experimental observations. This was different from that observed by Deegan et al. (*22*), who found three-dimensional clustering, but nonetheless mimics what was observed experimentally when spherical microcapsules were used. Neutrally buoyant capsules of different sizes travel at the same velocity. Smaller capsules penetrate closer to the drop perimeter edge before eventually succumbing to the interfacial force strength once a portion of the capsule extends beyond the water/air interface. Larger capsules succumb to the interfacial force before smaller capsules as both approach the pinned contact line due to the curvature and depth of the carrier drop along the edge.

Drop size has a critical role in annular ring formation and capsule clustering. A drop of water containing a known microcapsule concentration (2 μm capsule size distribution) was placed on a glass slide and only the drop size was allowed to vary. The larger drop takes longer to evaporate and affects capsule clustering at the wetted perimeter, which ultimately increases capsule transport to the drop edge. This observation was not readily anticipated due to the larger length scale associated with the larger droplet (e.g., more time for the drop to evaporate but also a longer length scale for the microcapsules to be transported to the drop pinned edge).

Figure 11 represents multiple observations for the 2 μm blank formulation as a function of capsule density and water drop size for capsule clusters at/near the wetted perimeter contact line. Only a portion of the contact perimeter is provided in the photographs. Capsule concentrations are relative, beginning with 4×, followed by a 2× dilution with water, and so on, to yield different initial capsule concentrations within the water drop. The coffee stain effect for microcapsules was altered by both capsule density and drop size for the water carrier. Annular rings of microcapsules were observed as the carrier drop size decreased and/or the number density of capsules within the drop increased. Numerical approaches used to predict pesticide release rates from
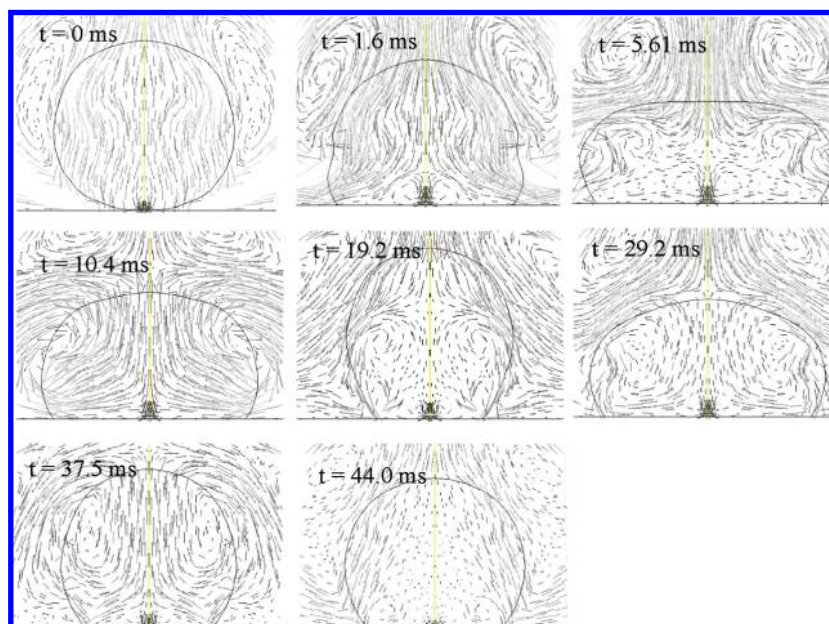
Figure 8. Velocity vectors within and surrounding an impinging water droplet on a simulated leaf surface. Contact angle constraint = 135°.

Figure 9. Capsule particle size distribution for mixtures labeled as either 2 or 10 μm blanks.

Figure 10. Example of blank 10 μm (average diameter) capsule clusters near a portion of wetted perimeter edge following drop drying, looking down onto the solid surface.
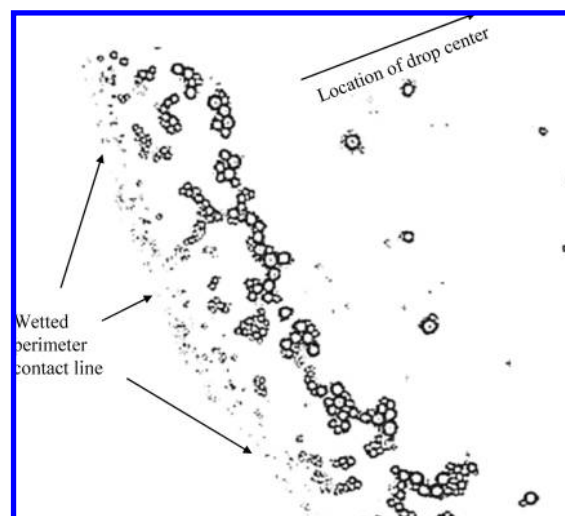
single capsules would overpredict losses from clustered microcapsules.

Drop Evaporation Rate. Mass loss for pure water droplets (evaporation) was linear over time as measured by TGA. This linear rate of mass loss yields the rate of volume change (dV/dt) and height (dh/dt) of the evaporating drop which was used with eqs 6−8 to calculate convective flow fields within the drop.

Time for Droplet Evaporation as a Function of Drop Size. The evaporation rate of water was sufficiently small that a quasi-static approximation for the dynamic behavior for changes in drop shape during evaporation is valid. The change in the spherical cap height with respect to the scaled time (t/t_f) for a sessile drop having a pinned contact line is linear under quasi-static assumptions.

$$\frac{dh}{d(t/t_f)} \cong h_0 \qquad (19)$$

Only for contact angles $\geq 90°$ do small deviations from linearity arise. Thus, the rate of mass loss is proportional to the height of the spherical cap (*38*), and not the spherical radius.

Velocity Profile Derived from Spherical Cap Approximation. *Convective Velocity Magnitude During Evaporation.* Velocity magnitudes were small near the drop center and increased near the pinned contact line edge. The two-dimensional nature of the velocity profile becomes one-dimensional as the drop evaporates and the lubrication theory assumptions become valid. Analytical solutions involving an infinite series often converge after a finite number of terms are collected. The number of terms in the Legendre polynomial required before the velocity magnitude converges to its final value was ~60.

Quantitative Velocity Observations. Comparison of theory (*22*, *35*) with experimental observations of velocity magnitudes for a 5 μL evaporating drop is provided in **Figure 12** for $t/t_f = 0.5$ and $\theta_0 = 25°$. Similar order of magnitude comparisons were found, especially near the wetted perimeter where velocity magnitudes were largest.

Capsule Clustering (Coffee Stain). Observations illustrate microcapsules were transported from the bulk liquid to the wetted perimeter as the surrounding carrier fluid evaporates. The force
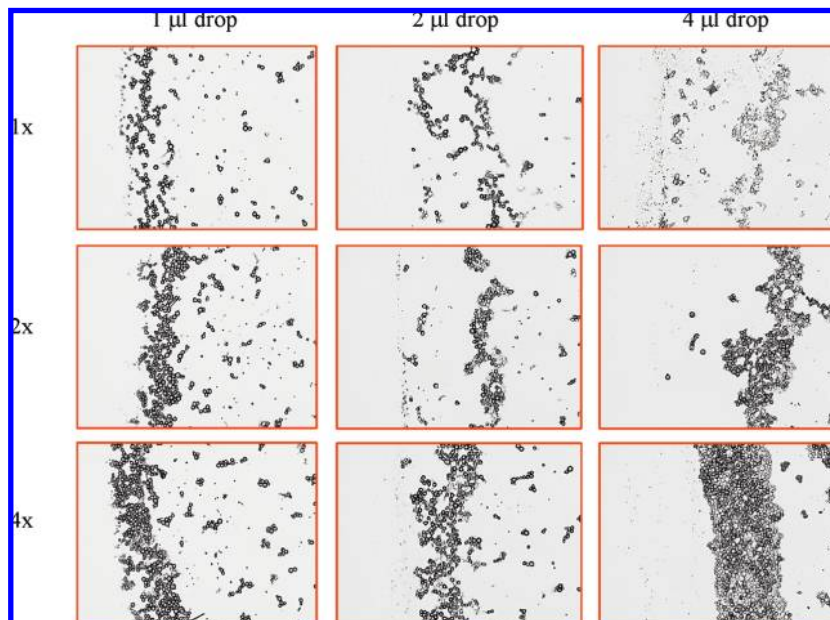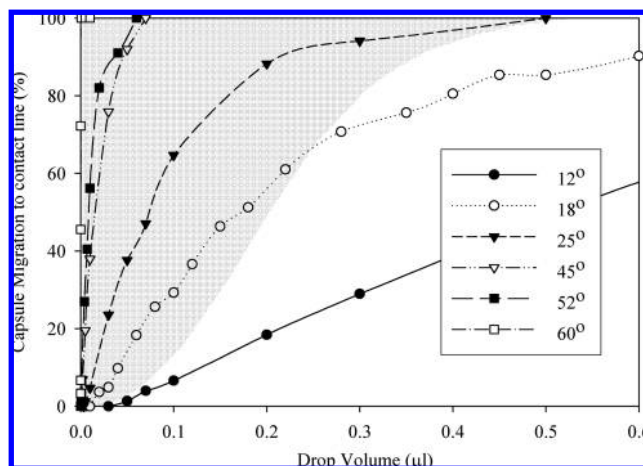
Figure 11. Comparison of the effect of the annular ring of capsules upon drop evaporation as a function of drop volume and capsule concentration. 1x is the reference concentration (thus, $4\times$ has 4 times as many capsules in the same drop volume).
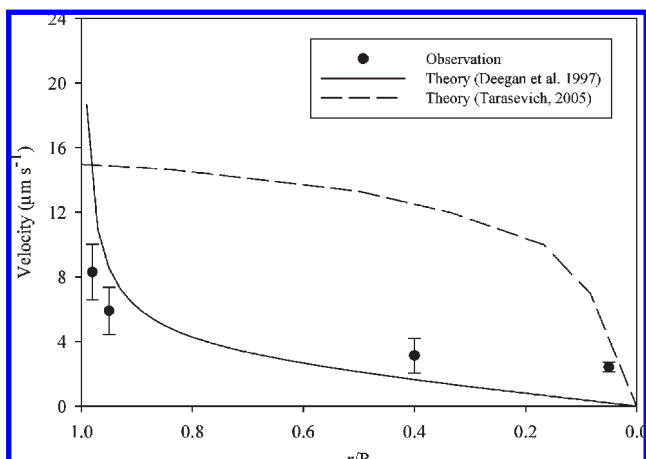
Figure 12. Velocity magnitudes from evaporating a 5 μL drop on a glass slide containing microcapsules (2 μm).

Figure 13. Percentage of uniformly dispersed microcapsules predicted to migrate to pinned contact line following solvent evaporation as a function of initial contact angle. Shaded area represents agricultural nozzle droplet sizes classified from very fine to coarse.

balance coupled with the quasi-static assumptions and potential flow velocity profile (eqs 6−8) was written in Visual Basic for Applications (VBA) and evaluated numerically. Microcapsules were uniformly placed in the drop at the onset of evaporation ($t/t_f = 0$) as an initial condition for the simulation, and these capsules were numerically tracked over time. Capsule (x,y) locations and the interface shape were solved for and written at each time step. The numerical system was executed for different drop sizes (initial contact angle of 25°), all having the same microcapsule density. Estimates of the width of the annular ring clustering of microcapsules were obtained by knowing the microcapsule sizes and concentrations along with the droplet size and contact angle.

The larger drops typically have 100% of the initial uniformly distributed microcapsules transported to the pinned, wetted perimeter edge upon evaporation (**Figure 13**). The percentage of microcapsules reaching the wetted perimeter edge before the drop fully evaporates decreases as the water drops decrease in volume. There is a competition between microcapsule transport and drop evaporation. The quasi-static mathematical description suggests microcapsule transport, and the formation of the annular ring

was a function of initial drop size, equilibrium contact angle, and, perhaps, the initial locations of microcapsules within the sessile drop as the drop initially comes to rest.

The droplet size distributions for conventional agricultural nozzles (shaded area, **Figure 13**) represent the very fine to coarse droplet size distribution classes obtained from atomization experiments (*39*). Thus, all spray nozzles of agricultural importance yield drop diameters of sufficient size so that a portion of the microcapsules with these carrier drops will cluster near the perimeter edge (seen experimentally and predicted numerically). It was anticipated that most if not all droplets created by agricultural nozzles are within the transition regimen where the "doughnut" monolayer cluster of capsules can be significant, with the width of the cluster (and thus pesticide release rate) given by the initial drop volume and the contact angle with the solid surface, along with conventional parameters that govern Fickian diffusion.

Parameters Characterizing Pesticide Release Rates. Observations and model predictions indicate quantification of microcapsule

5450 *J. Agric. Food Chem.,* Vol. 57, No. 12, 2009

Cryer and Wilson

Table 2. Parameters Known To Affect Microcapsule Release Rate, Efficacy, and Environmental Behavior

traditional	new
pesticide loading	capsule size (for cluster width)
polymer (for encapsulation)	capsule size distribution
polymer membrane thickness	capsule density in drop
capsule size	solvent evaporation rate
	sessile drop wetted contact area
	sessile drop contact angle

clustering is required for refined efficacy and environmental knowledge regarding pesticide release rates, in addition to conventional parameters that affect release such as microcapsule size and polymer membrane properties (**Table 2**). The modeling approach outlined in this paper provides a mechanism to deduce capsule clustering and the impact clusters have on the overall pesticide release rate. Thus, optimal release patterns can be constructed to yield the desired biological effect that combines both formulation characteristics and application parameters (e.g., drop size, contact angle) because they are not mutually exclusive.

Experimental observations of microcapsule placement following drop (water) evaporation illustrate capsule cluster monolayers were generated at the former (original) pinned contact line of the drop. CFD simulations suggest solid particles within the drop are pushed to the exterior contact line during drop impact with the solid surface, which may be partially responsible for the pinned contact line once the sessile drop becomes stationary. The radius of the pinned contact line is a function of both the solvent/solid contact angle and the drop size/volume. Surface tension affects the starting shape of the sessile drop and thus can affect capsule movement and possibly clustering during evaporation.

Capsule clustering is predicted to occur across all drop sizes of relevance for agricultural nozzles, and the width of the capsule cluster ring is a function of the initial drop size, capsule number density, and the initial (equilibrium) contact angle of the resulting sessile drop. Microcapsules are more likely to be deposited in a uniform pattern as the drop size decreases.

Capsule clustering and the impact on pesticide release rate have largely been historically ignored, with researchers focusing on algorithms to describe diffusion processes for single capsules. Often, a formulation that works under greenhouse and laboratory conditions fails when taken to the field. Microcapsule transport mechanisms in the evaporating sessile drop may provide a mechanism to address failure rates partially attributed to reduced pesticide release (and thus efficacy) resulting from capsule clustering. Conventional microcapsule attributes and the self-assembly of microcapsule clustering in evaporating sessile drops can now be used to predict environmental concentrations of pesticides following release.

The quasi-static approach to model the dynamic behavior of the sessile drop shape during evaporation proved to be adequate to address observed clustering of microcapsules. A semiempirical diffusion model was developed for estimating pesticide release loss from two-dimensional clusters of microcapsules. Predicted environmental release patterns are combinations of various capsule size distributions and geometries, polymer membrane thickness, pesticide loading, and environmental dissipation parameters. This coupling of microcapsule formulation attributes, formulation design, and capsule placement, with biological observations, can increase the likelihood for formulation success under field conditions. Properly accounting for physical phenomena such as microcapsule clustering and their impact on pesticide release rate reduces efficacy uncertainty and

the likelihood for undesirable behavior under a variety of different conditions.

LITERATURE CITED

(1) Kydonieus, A. F. Fundamental concepts of controlled release. *Controlled Release Technologies: Methods, Theory, and Applications*; Kydonieus, A. F., Ed.; CRC Press: Boca Raton, FL, 1980; Vol. I, pp 1−19.

(2) Cowsar, D. R. Controlled release: benefits vs. risks. *Controlled Release of Pesticides and Pharmaceuticals*; Lewis, D. H., Ed.; Plenum Press: New York, 1981.

(3) Mogul, M. G.; Akin, H.; Hasirci, N.; Trantolo, D. J.; Gresser, J. D.; Wise, D. L. Controlled release of biologically active agents for purposes of agricultural crop management. *Resources, Conservation Recycling* **1996**, *16*, 289−320.

(4) Akelah, A. Novel utilizations of conventional agrochemicals by controlled release formulations. *Mater. Sci. Eng. C* **1996**, *4*, 83−98.

(5) Green, J. M.; Beestman, G. B. Recently patented and commercialized formulation and adjuvant technology. *Crop Prot.* **2007**, *26*, 320−326.

(6) Greene, L. C.; Meyers, P. A.; Springer, J. T.; Banks, P. A. Biological evaluation of pesticides released from temperature-responsive microcapsules. *J. Agric. Food Chem.* **1992**, *40*, 2274−2278.

(7) Dailey, O. D.; Dowler, C. C.; Mullinix, B. G. Polymeric microcapsules of the herbicides atrazine and metribuzin: preparation and evaluation of controlled-release properties. *J. Agric. Food Chem.* **1993**, *41*, 1517−1522.

(8) Dowler, C. C.; Dailey, O. D.; Mullinix, B. G. Polymeric microcapsules of alachlor and metolachlor: preparation and evaluation of controlled-release properties. *J. Agric. Food Chem.* **1999**, *47*, 2908−2913.

(9) Quaglia, F.; Barbato, F.; De Rosa, G.; Granata, E.; Miro, A. ; Imacolata La Rotonda, M. Reduction of the environmental impact of pesticides: waxy microspheres encapsulating the insecticide carbaryl. *J. Agric. Food Chem.* **2001**, *49*, 4808−4812.

(10) Dailey, O. D. Volatilization of alachlor from polymeric formulations. *J. Agric. Food Chem.* **2004**, *52*, 6742−6746.

(11) Asrar, J.; Ding, Y.; La Monica, R. E.; Ness, L. C. Controlled release of tebuconozole from a polymer matrix microparticle: release kinetics and length of efficacy. *J. Agric. Food Chem.* **2004**, 52, 4814−4820.

(12) El Bahri, Z.; Taverdet, J.-L. Elaboration and characterisation of microparticles loaded by pesticide model. *Powder Technol.* **2007**, *172*, 30−40.

(13) Allan, G. G.; Chopra, C. S.; Neogi, A. N.; Wilkins, R. M. Design and synthesis of controlled release pesticide−polymer combinations. *Nature* **1971**, *234*, 349−351.

(14) Collins, R. L.; Doglia, S. Concentration of pesticides slowly released by diffusion. *Weed Sci.* **1973**, *21*, 343−349.

(15) Crank, J. *The Mathematics of Diffusion*, 2nd ed.; Clarendon Press: Oxford, U.K., 1993.

(16) Carslow, H. S.; Jaeger, J. C. *Conduction of Heat in Solids*; Clarendon Press: Oxford, U.K., 1959.

(17) Roseman, T. J.; Cardarelli, N. F. Monolithic polymer devices. *Controlled Release Technologies: Methods, Theory, and Applications*; Kydonieus, A. F., Ed.; CRC Press: Boca Raton, FL, 1980; Vol. I, pp 21−54.

(18) Bahadir, M.; Pfister, G. *Controlled Release Formulations of Pesticides. Chemistry of Plant Protection. Controlled Release, Biochemical Effects of Pesticides, Inhibition of Plant Pathogenic Fungi. 6*; Bowers, W. S., Ebing, W., Martin, D., Wegler, R., Eds.; Springer: New York, 1990; pp 1−64.

(19) Siepmann, J.; Peppas, N. A. Modeling of drug release from delivery systems based on hydroxypropyl methylcellulose (HPMC). *Adv. Drug Delivery Rev.* **2001**, *48*, 139−157.

(20) Muro-Sune, N.; Gani, R.; Bell, G.; Shirley, I. Predictive property models for use in design of controlled release of pesticides. *Fluid Phase Equilib.* **2005**, *228−229*, 127−133.

(21) Muro-Sune, N.; Gani, R.; Bell, G.; Shirley, I. Model-based computer-aided design for controlled release of pesticides. *Comput. Chem. Eng.* **2005**, *30*, 28−41.

(22) Deegan, R. D.; Bakajin, T. F.; Dupont, G.; Huber, S. R.; Nagel, T.; Witten, A. Capillary flow as the cause of ring stains from dried liquid drops. *Nature* **1997**, *389*, 827.

(23) Widjaja, E.; Harris, M. T. Particle deposition study during sessile drop evaporation. *AIChE J.* **2008**, *54*, 9, 2250−2260.

(24) Hu, H.; Larson, R. G. Evaporation of a sessile droplet on a substrate. *J. Phys. Chem. B* **2002**, *106*, 1334−1344.

(25) Kondic, L.; Murisic, N. On modeling evaporation of sessile drops. Presented at the AIChE Annual Meeting, Philadelphia, PA, Nov 16−21, 2008.

(26) Maillard, M.; Motte, L.; Pileni, M. P. Rings and hexagons made of nanocrystals. *Adv. Mater.* **2001**, *13* (3), 200−204.

(27) Small, W. R.; Walton, C. D.; Loos, J.; in het Panhuis, M. Carbon nanotube network formation from evaporating sessile drops. *J. Phys. Chem. B* **2006**, *110*, 13029−13036.

(28) Dufresne, E. R.; Corwin, E. I.; Greenblatt, N. A.; Ashmore, J.; Young, D. Y.; Dinsmore, A. D.; Cheng, J. X.; Xie, X. S.; Hutchinson, J. W.; Weitz, D. A. Flow and fracture in drying nanoparticle suspensions. *Phys. Rev. Lett.* **2003**, *91*, 224501.

(29) Tsukruk, V. V.; Ko, H.; Peleshanko, S. Nanotube surface arrays: weaving, bending, and assembling on patterned silicon. *Phys. Rev. Lett.* **2004**, *92*, 065502.

(30) Smalyukh, I. I.; Zribi, O. V.; Butler, J. C.; Lavrentovich, O. D.; Wong, G. C. L. Structure and dynamics of liquid crystalline pattern formation in drying droplets of DNA. *Phys. Rev. Lett.* **2006**, *96*, 177801.

(31) Hu. H.; Larson, R. G. Marangoni effect reverses coffee-ring depositions. *J. Phys. Chem. B* **2006**, *110*, 7090−7094.

(32) Deegan, R. D.; Bakajin, O.; Dupont, T. F.; Huber, G.; Nagel, S. R.; Witten, T. A. Contact line deposits in an evaporating drop. *Phys. Rev. E* **2000**, *62* (1), 756−765.

(33) Popov, Y. O. Singularities, universality, and scaling in evaporative deposition patterns. Ph.D. Dissertation, Department of Physics, University of Chicago, Chicago, IL, 2003.

(34) Popov, Y. O. Evaporative deposition patterns: spatial dimensions of the deposit. *Phys. Rev. E* **2005**, *71*, 036313.

(35) Tarasevich, Y. Y. Simple analytical model of capillary flow in an evaporating sessile drop. *Phys. Rev. E* **2005**, *71*, 027301.

(36) ANSYS, Inc. Fluent computational fluid dynamics software, Santa Clara, CA, 2006.

(37) Brakke, K. A. The surface evolver. *Exp. Math.* **1992**, *1* (2), 141−165.

(38) Rowan, S. M.; Newton, M. I.; McHale, G. Evaporation of microdroplets and the wetting of solid surfaces. *J. Phys. Chem.* **1995**, *99*, 13268−13271.

(39) Doble, S. J.; Mathews, G. A.; Rutherford, I.; Southcombe, E. S. E. A system for classifying hydraulic nozzles and other atomizers into categories of spray quality. *Proc. Br. Crop Prot. Conf., Weeds* **1985**, *3*, 1125−1133.